Antiviral Research 168 (2019) 36–50

Contents lists available at ScienceDirect

Antiviral Research

journal homepage: www.elsevier.com/locate/antiviral

Mitophagy in human astrocytes treated with the antiretroviral drug Efavirenz: Lack of evidence or evidence of the lack

Olga Martinez-Arroyo[a], Aleksandra Gruevska[a], Victor M. Victor[b,c,d], Rosa A. González-Polo[e,f,g], Sokhna M.S. Yakhine-Diop[e,f,g], Jose M. Fuentes[e,f,g], Juan V. Esplugues[a,b,c], Ana Blas-Garcia[a,b,i,1], Nadezda Apostolova[a,b,*,1]

[a] Departamento de Farmacología, Facultad de Medicina, Universidad de Valencia, Valencia, Spain
[b] Centro de Investigación Biomédica en Red de Enfermedades Hepáticas y Digestivas (CIBERehd), Spain
[c] FISABIO–Hospital Universitario Dr. Peset, Valencia, Spain
[d] Departamento de Fisiología, Facultad de Medicina, Universidad de Valencia, Valencia, Spain
[e] Departmento de Bioquímica, Biología Molecular y Genética, Facultad de Enfermería y Terapia Ocupacional, Universidad de Extremadura, Cáceres, Spain
[f] Centro de Investigación Biomédica en Red sobre Enfermedades Neurodegenerativas (CIBERNED), Cáceres, Spain
[g] Instituto Universitario de Investigación Biosanitaria de Extremadura (INUBE), Spain
[i] Departamento de Ciencias Biomédicas, Universidad Europea de Valencia, Valencia, Spain

ARTICLE INFO

Keywords:
Autophagy
Mitophagy
Efavirenz
Mitochondria
Antiretroviral

ABSTRACT

Efavirenz (EFV), a first generation non-nucleoside analogue reverse transcriptase inhibitor widely employed in combination antiretroviral therapy regimens over the last 20 years, has been associated with a wide range of neuropsychiatric effects and has also been linked with HIV-associated neurocognitive disorder (HAND). EFV has been reported to alter mitochondrial dysfunction and bioenergetics in different cell types, including astrocytes. Here, we analyzed whether this mitochondrial effect is associated with alterations in autophagy and, more specifically, mitophagy. U251-MG cells were exposed to EFV (10 and 25 μM; 24 h) and the effect was compared with that of CCCP - an uncoupler of the mitochondrial membrane potential and widely-employed *in vitro* inducer of mitophagy – and those of the known pharmacological stressors rotenone and thapsigargin, selected due to reported similarities with EFV. EFV induces autophagy with functional autophagic flux despite the accumulated p62/SQSTM1. However, it fails to activate canonical mitophagy (according to mitochondrial mass and expression of mitophagy-related proteins). The fact that EFV-exposed cells display decreased levels of TOM20, an outer mitochondrial membrane protein, together with the association of TOM20 with autophagosomes (LC3), points to an alternative form of mitochondrial degradation. Moreover, the perinuclear mitochondrial cluster in EFV-treated cells differs from that displayed with CCCP. Also, in EFV-treated cells, p62 was associated with mitochondria, which may be related to the mito-protective function of this autophagic protein. In conclusion, these findings add to the existing knowledge of the EFV-triggered mitochondrial interference, a mechanism that may be implicated in the adverse CNS events observed in the clinics.

1. Introduction

Among the available anti-HIV drugs, the first generation non-nucleoside analogue reverse transcriptase inhibitor (NNRTI) Efavirenz (EFV), is associated with the greatest level of CNS toxicity (Apostolova et al., 2015a), and has been linked to a decline of neurocognitive function in HIV patients (Ma et al., 2016). Although the dominant position of EFV within initial combined antiretroviral therapy (cART) has recently been challenged by the arrival of newer antivirals with better safety, which has relegated EFV to being an alternative treatment as suggested by the majority of cART guidelines, EFV is still used in many countries and takes part of the treatment of choice for specific patients.

Abbreviations: ABC, abacavir; EFV, Efavirenz; ETC, electron transport chain; HIV, human immunodeficiency virus; $\Delta\Psi_m$, mitochondrial membrane potential; NNRTI, non-nucleoside reverse transcriptase; RVP, rilpivirine; OMM, outer mitochondrial membrane; OXPHOS, oxidative phosphorylation; ROS, reactive oxygen species; Rot, rotenone; TG, thapsigargin

* Corresponding author. Avda Blasco Ibañez n.15-17, 46010, Valencia, Spain.
E-mail address: nadezda.apostolova@uv.es (N. Apostolova).

[1] these authors have contributed equally.

https://doi.org/10.1016/j.antiviral.2019.04.015
Received 3 January 2019; Received in revised form 11 April 2019; Accepted 30 April 2019
Available online 08 May 2019
0166-3542/

Despite the achievement of HIV treatment to greatly improve the health status of HIV-infected individuals, including a significant reduction in the burden of neurocognitive deficiency (Clifford and Ances, 2013), HIV-associated neurocognitive disorder (HAND) remains a major cause of morbidity affecting up to 50% of patients. Moreover, the necessity of chronic cART has led to various long-term complications including numerous CNS side effects (Carr and Cooper, 2000: Abers et al., 2014; Shah et al., 2016). The mechanisms underlying these actions have not yet been fully elucidated, but accumulated evidence obtained by several groups, including ours, highlights the capacity of EFV to interfere with mitochondrial function and to alter brain cellular bioenergetics (Streck et al., 2011; Purnell and Fox, 2014; Funes et al., 2014).

Oxidative phosphorylation (OXPHOS) and glycolysis are the main ATP-generating pathways in mammalian cells. Neurons rely mainly on OXPHOS; they divert glucose away from glycolysis to fuel the pentose phosphate pathway in order to maintain high levels of reduced glutathione (Magistretti and Allaman, 2018) and consequently are particularly vulnerable to mitochondrial damage. Conversely, astrocytes, the most abundant brain cell type, display active glycolysis, which is further enhanced under energetic stress. We observed this phenomenon in cultured cells exposed to clinically relevant concentrations of EFV. Both cell types displayed reduced O_2 consumption, with a direct and reversible inhibitory action on Complex I of the electron transport chain (ETC); increased mitochondrial superoxide production; and diminished mitochondrial membrane potential ($\Delta\Psi_m$) (Funes et al., 2014). However, unlike neurons, astrocytes increased ATP generation through glycolysis and thus proved less vulnerable. All evaluations were performed in both human cancer cell lines and rat primary cultures of astrocytes or neurons, rendering very similar results, for which we believe that the action of EFV on U251-MG is not related to the cancerous nature of the cell line employed.

Autophagy (or more precisely macroautophagy) is an evolutionarily conserved process in which intracellular components are engulfed in a double membrane vesicle (autophagosome) and further degraded in the lysosome (Choi et al., 2013). Increasing evidence suggests that autophagy is a protective mechanism in the brain, as it maintains the optimal balance and recycling of cellular resources. Mitophagy is a specialized autophagic process that disposes of dysfunctional mitochondria in order to maintain their overall integrity, the fine-tuning of their numbers and to provide the necessary components for their regeneration (Kim et al., 2007; Tolkovsky, 2009; King and Plun-Favreau, 2017). In healthy mammalian cells, mitophagy is an infrequent event and damaged mitochondria are repaired by fusion with functional mitochondria. However, when mitochondria are too heavily damaged to be repaired, their toxic accumulation is avoided by mitophagy, the only mechanism capable of eliminating whole mitochondria. Mitochondrial effector proteins can initiate two mitophagy pathways: the ubiquitin- and receptor-mediated (molecules containing LC3-interacting regions or LIRs). Ubiquitin-dependent mitophagy, the most widely understood form of signaling, is mediated by the coordinated activities of the mitochondrial serine-threonine kinase PTEN-induced putative kinase 1 (PINK1) and Parkin, an E3 ligase (called the Pink/Parkin pathway) (King and Plun-Favreau, 2017; Narendra et al., 2010). Accumulation of PINK1 on the outer mitochondrial surface triggers the kinase-dependent recruitment and activation of Parkin, which promotes ubiquitin conjugation and sequestosome 1 (SQSTM1)/p62-mediated recognition of target proteins within the outer mitochondrial membrane (OMM). The classical stimulus of Parkin-dependent mitophagy is the $\Delta\Psi_m$ loss achieved experimentally *in vitro* with high concentrations of the mitochondrial uncoupler carbonyl cyanide m-chlorophenyl hydrazone (CCCP) (King and Plun-Favreau, 2017). OMM LIR-containing proteins, or so-called mitophagy receptors such as NIX1 (also known as BNIP3L), BNIP3 (BCL-2 and adenovirus E1B 19-kDa-interacting protein 3), and FUNDC1 (FUN14 domain containing 1) trigger mitophagy under different conditions (Novak et al., 2010).

Numerous studies support the participation of astrocytes in HIV-associated neurotoxicity and HAND (Ton and Xiong, 2013). Given the peculiar cellular distribution of mitochondria in astrocytes, and their key role in energy metabolism, it is reasoned that they may directly participate in the metabolic changes associated with neuroinflammation, including that present in HIV infection. In astrocytes directly exposed to proinflammatory mediators, mitochondrial dynamics is altered and autophagy including mitophagy plays a role in maintaining mitochondrial homeostasis. In a very recent paper, it was shown that astrocytes productively infected with HIV-1 survive despite displaying mitochondrial injury due to increased mitochondrial fission and elimination of damaged mitochondria by mitophagy while on the contrary, bystander uninfected or unproductively infected astrocytes exhibit inflammasome activation and die by pyroptosis (Ojeda et al., 2018). In addition, astrocytes are in close physical and functional contact with neurons, and there is evidence of astrocytes phagocyting axonal mitochondria from adjacent neurons in a process called “transcellular mitophagy” (Davis et al., 2014). Whether this phenomenon has any link with HIV infection and CNS side effects or HAND is unknown. In summary, the implication of astrocytes in HAND and in particular the pathophysiological processes related to mitochondria in these cells are relevant and merit in-depth research.

We and others have already shown that EFV triggers autophagy in several cell types *in vitro*, including neurons (Purnell and Fox, 2014; Apostolova et al., 2011; Dong et al., 2013; Weiβ et al., 2016) but there is still a lack of information regarding astrocytes. In addition, there is no conclusive evidence of the potential of EFV to modulate mitophagy. Given the mitochondrial effect of EFV in glial cells and the peculiarities of mitochondrial function in this cellular population, we aimed to analyze whether EFV induces autophagy and, in particular, mitophagy using the same experimental model previously described (Funes et al., 2014).

2. Material and methods

2.1. Reagents and treatments

Unless stated otherwise, chemicals were obtained from Sigma-Aldrich. Antiretroviral drugs - EFV, Abacavir (ABC) and Rilpivirine (RPV) - were from Sequoia Research Products and were dissolved in DMSO (EFV, stock of 25 mM, and RPV, stock of 1 mM) or water (ABC, stock of 1 mM). They were employed at clinically relevant plasma concentrations- EFV (10 and 25 μM), RPV (0.25, 0.5 and 1 μM) and ABC (5, 10 and 25 μM).

2.2. Cell line and treatments

We employed the human immortalized glioma cell line U251-MG (CLS 300385, European Collection of Cell Culture). Cell cultures were maintained and treated as described previously (Funes et al., 2014). Some experiments were also performed in primary cultures of astrocytes obtained from cerebral cortex of 24 h-old Wistar rat neonates (Funes et al., 2014). Isolated cells were plated (1.2×10^5 cells/cm^2) in DMEM supplemented with 10% FBS and cultured for 12–14 days. Under these conditions, astrocytes represented 85% of the cells, the remaining proportion being microglia and progenitor cells. The protocols regarding isolation and primary cell culture were approved by the Ethics Committee of the University of Valencia and complied with European Community guidelines for the use of animal experimental models.

EFV was employed at clinically relevant plasma concentrations (10 and 25 μM) similar to those employed by other groups (Arendt et al., 2016) and chosen due to the fact that EFV presents very high plasma protein binding capacity (> 99%) and displays great interpatient variability in its plasma levels being these supratherapeutic in as many as 40% of the patients in some studies (Apostolova et al., 2015b). EFV was compared to similar pharmacological modulators: thapsigargin

(TG), the classic inhibitor of the Ca^{2+} transporter SERCA, which, like EFV, has the property of being an ER stress inducer and has also been described as a modulator of autophagy (TG, 2 μM) (Zhang et al., 2014), and two mitochondrial stressors: rotenone (Rot, 10 μM), a common pharmacological inhibitor of Complex I of the ETC and a producer of mitochondrial superoxide; and CCCP (10 μM), a known activator of the mitophagy (Shi et al., 2015). This subtoxic concentration of CCCP was employed in order to preserve cell viability and in addition, to avoid induction of massive (non-selective) autophagy. Additionally, we used a vehicle control (DMSO) and a negative control (untreated cells). For the study of autophagic flux, cells were pre-treated with bafilomycin A1 (20 nM, 1 h), a macrolide antibiotic employed as a selective and potent inhibitor of the vacuolar-type ATPase (V-ATPase), which inhibits autophagy by preventing fusion between autophagosomes and lysosomes, and thus impairing the recycling of LC3-II for new phagophores (Yamamoto et al., 1998).

2.3. Evaluation of protein expression analysis by Western blotting

Whole cell protein extracts were obtained, quantified and immunoblotted as described elsewhere (Funes et al., 2014). Immunolabelling was detected using the chemiluminescent substrate LuminataTM Crescendo or Forte (Merck Millipore), and was visualized with a digital luminescent image analyser (FUJIFILM LAS 3000, Fujifilm). Multi Gauge software version 3.0. was used for densitometric analysis. Primary antibodies: anti-Actin (rabbit polyclonal, 1:1000), anti-SQSTM1/p62 (for the experiments in U251-MG, mouse monoclonal, 1:1000), anti-Parkin (mouse polyclonal, 1:500) from Santa Cruz Biotechnology; anti-SQSTM1/p62 (for the experiments in primary rat astrocytes, mouse monoclonal, 1:1000, Abnova) and anti-TOM20 (rabbit polyclonal, 1:1000, Proteintech); anti-PINK1, anti-MAVS, anti-VDAC1, anti-HADHA (all rabbit polyclonal), and anti-Clpx (rabbit monoclonal) (all used at 1:1000, from Abcam); anti-LC3 (rabbit polyclonal, 1:1000, Sigma-Aldrich) and anti-ACO2 (rabbit polyclonal, 1:1000, Abnova). Secondary antibodies: peroxidase-labelled anti-mouse (1:2000, Thermo Fisher Scientific) and anti-rabbit IgG (1:5000, Vector laboratories).

2.4. Evaluation of mRNA levels by quantitative RT-PCR

Total RNA was extracted (RNeasy Mini Kit, Qiagen), eluted (30 μL of water) and quantified (NanoDropR ND-1000 spectrophotometer, NanoDrop Technologies). Next, complementary DNA (cDNA) was synthetized (2 μg of total RNA) using the "PrimeScriptTM RT Reagent Kit" (TaKaRa Bio Inc.) in a final volume 20 μL and the presence of PrimeScript Buffer, 1 μL PrimeScript RT Enzyme Mix I, 25 pmol Oligo dT Primer and 50 pmol random sexamers in a GeneAmp® PCR System 2400 (PerkinElmer) under the following conditions: 37 °C (15 min), 85 °C (5 s) and 4 °C (∞). Finally, qRT-PCR was performed with SYBR® Premix Ex Taq™ (Tli RNaseH Plus) (TaKaRa Bio Inc.), containing TaKaRa Ex Taq HS, dNTP mixture, Mg^{2+}, Tli RNase H and SYBR Green I. The reaction was performed mixing 1 μL cDNA, 5 μL SYBR® Premix Ex Taq™, 2 μM primers (forward and reverse, details in Supplementary Table 1) and RNase-free water (10 μL final volume) using a Lightcycler® 96 Real-Time PCR System (Roche Life Science). Experiments were performed in duplicate, yielding a value for a biological replicate, together with a negative control (RNase-free water instead of cDNA).

2.5. Assessment of mitochondria, lysosomes and autophagosomes by confocal fluorescence microscopy

We used a Leica TCS-SP2 confocal laser scanning unit (Leica Microsystems) with argon and helium-neon laser beams, attached to a Leica DMIRBE inverted microscope (at Unidad Central de Investigación de Medicina, UCIM, Universidad de Valencia, Valencia, Spain). Images were captured at 63× (HCX PL APO 40.0 × 1.32 oil UV) or 40× magnification (HC PL APO 40×/1.30 Oil PH3 CS2 objective). Treatments (24 h) were performed with 25,000 cells/well, cultured on chambered borosilicate coverglasses (Nunc™ Lab-Tek™ Chambered Coverglass, Thermo Fisher Scientific) and included EFV (10 and 25 μM), Rot 10 μM, CCCP 10 μM and TG 2 μM. In the case of live-cell imaging, 0.1 μM LysoTracker Green or 1 μM MitoTracker Red (both from Thermo Fisher Scientific) were added for the last 30min of treatment. For p62 colocalization, cells were first stained with 0.5 μM Mitoview633 (Biotium) during the last 30 min of treatment. For immunocytochemistry experiments, cells were fixed with 4% formaldehyde (15 min), washed with PBS at pH 8.0 and blocked (1 h; 5% goat serum and 0.3% Triton X-100 in PBS). Cells were then incubated (overnight, 4 °C) with the primary antibodies anti-TOM20 (1:250), anti-LC3 (1:400) or anti-p62 (1:150), washed and incubated (1 h, RT) with the secondary antibodies goat anti-rabbit Alexa Fluor 488 or goat anti-mouse Alexa Fluor 594 (Thermo Fisher Scientific, 1 h, RT). Finally, Hoechst 33342 (5 μM) was added for the last 30min to stain the nuclei. Colocalization between two fluorescent signals was quantified using the programme Image J (Colocalization colormap plugin) using the method developed by Jaskolski (Jaskolski et al., 2005) which is a modification of intensity correlation analysis and permits the quantification of correlation while preserving the spatial information by evaluating pairs of individual pixels rather than between global images. This method provides us with a correlation index (Icorr) of the two signals and with normalized mean deviation product (nMDP). The latter ranges from −1 to 1, where negative values represent non-correlated and positive values indicate correlated pixels. The I_{corr} index represents the fraction of pixels with positive nMDP values.

2.6. Assessment of mitochondrial and lysosomal mass by flow cytometry

Cells were treated, detached by trypsin-EDTA (Sigma-Aldrich) and incubated (15 min, 37 °C) in complete medium containing 100 nM MitoTracker Green or 100 nM LysoTracker Red (both from Thermo Fisher Scientific) to analyze mitochondrial and lysosomal mass, respectively, by a flow cytometer (Beckman Coulter FC500-MPL). In the case of the measurement of mitochondrial mass, prior to treatment, cells were preloaded with 100 nM MitoTracker® Green FM (Thermo Fisher Scientific) for 15 min and PBS-washed.

2.7. Presentation of data and statistical analysis

Values are expressed as mean ± standard deviation (SD). The number of independent experiments (n) is indicated in the figure legends. Unless otherwise stated, data are represented as percentage of control (untreated cells considered 100%), a normalization performed in order to remove any unwanted sources of variation. Data were analyzed using GraphPad Prism® V6.01 (GraphPad Prism® Software Inc). Comparisons between two groups or with respect to control conditions were independently performed using a Student's *t*-test; statistical significance versus vehicle or untreated cells: $P < 0.05$ (*), $P < 0.01$ (**) or $P < 0.001$ (***).

3. Results

3.1. Activation of autophagy in U-251-MG cells exposed to EFV

The capacity of EFV to induce autophagy or mitophagy in U251-MG cells was explored at two clinically relevant concentrations (10 and 25 μM) and in comparison with several other stimuli chosen due to the similarities of their actions with those of EFV. As shown in Fig. 1A, 24 h-treatment with EFV25 enhanced the generation of autophagosomes, observed as increased LC3-II levels (Western blotting). Interestingly, TG incremented LC3-II expression, while Rot failed to do so. Evaluation at 8 h showed no changes in LC3 expression (data not shown) and therefore we performed further experiments at 24 h. LC3 exists in two forms:

LC3-I, cytosolic, and its product LC3-II, shorter for one amino acid, membrane-bound and lipidated. As LC3-II is part of the autophagosomal membrane, LC3-I-into-LC3-II conversion is a useful autophagy biomarker (Klionsky et al., 2016), nevertheless given certain controversies (Jiang and Mizushima, 2015), we quantified both total LC3-II and LC3-II/LC3-I ratio. The presence of LC3-II-associated punctae - characteristic of the formation of autophaghosomes - was confirmed in EFV-, TG- and CCCP-treated cells by confocal fluorescence

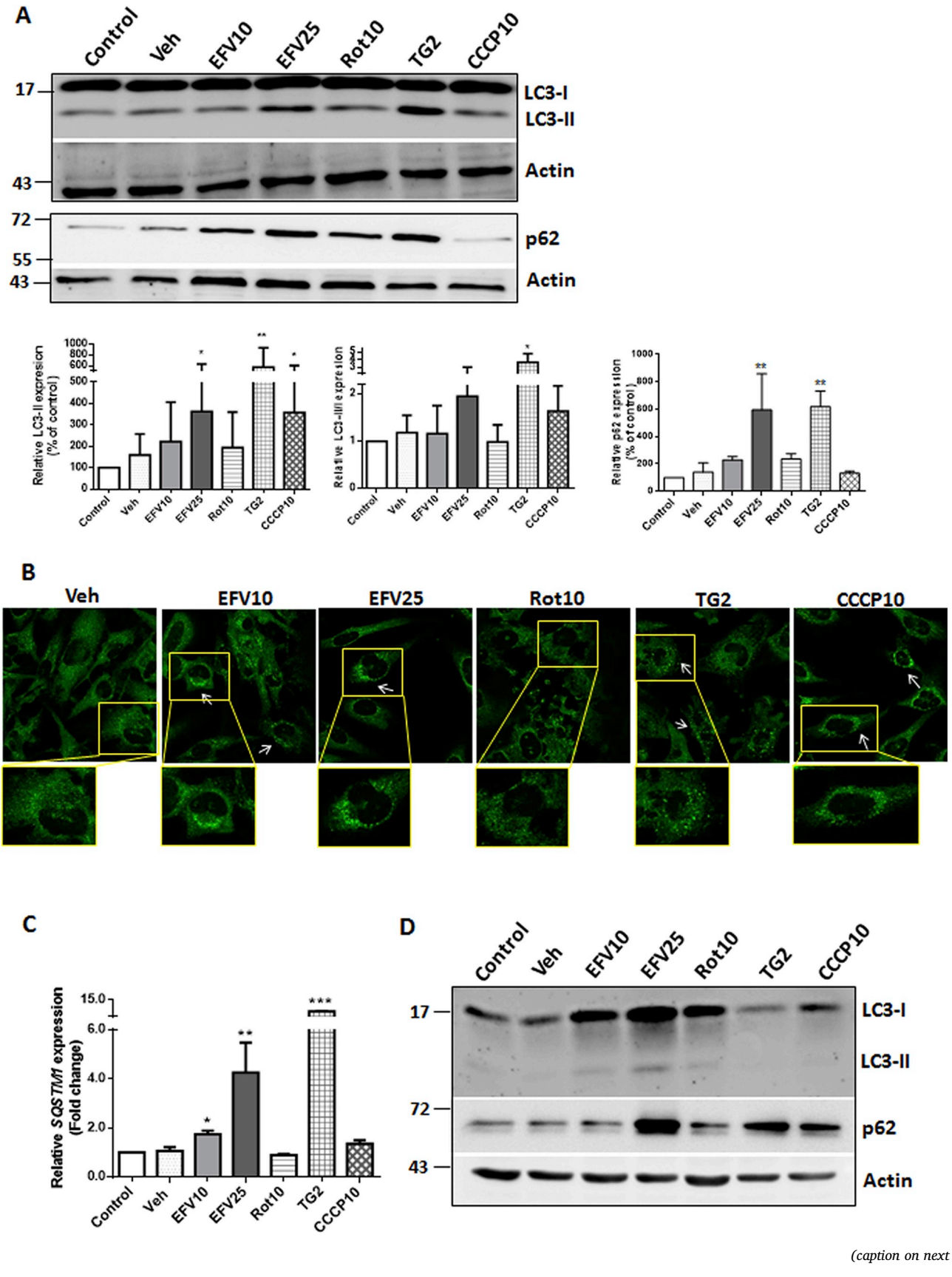

(caption on next page)

Fig. 1. Analysis of general markers of autophagy. Cells (U251-MG except for panel D, primary rat astrocytes) were treated for 24 h with efavirenz (EFV10 and 25 μM), vehicle (DMSO), thapsigargin (TG 2 μM), rotenone (Rot 25 μM) or CCCP 10 μM. **(A)** Immunoblot analysis of whole-cell protein extracts showing a representative Western blotting image and histograms expressing quantification of LC3-II and LC3-II/I ratio, and SQSTM1/p62 levels after normalization with the expression of the loading control, β-actin. Data are shown as mean ± SD, $n = 12$ for LC3 (except for CCCP, $n = 7$) and $n = 11$ for p62 (except for EFV10 and TG2, $n = 10$) are expressed as % of control (untreated cells, considered 100%). **(B)** Representative confocal fluorescence microscopy images of cells stained for LC3 (63× augmentation and images with an additional 2× digital zoom). Autophagosome-associated punctae are marked with an arrow. **(C)** Analysis of the mRNA level of *SQSTM1* by quantitative RT-PCR. Data (mean ± SD, $n = 3$ for Veh, EFV10 and TG2, and $n = 4$ for the rest) are expressed as mRNA content in relation to that of the control (untreated cells, considered 1) after normalization with the expression of the housekeeping gene *ACTB* (β-actin). **(D)** Immunoblot analysis of LC3 and p62 protein content in whole-cell extracts of primary rat astrocytes using β-actin as a loading control. Representative images are shown. **(E)** Immunoblot analysis of whole-cell protein extracts showing a representative Western blotting image and histograms expressing quantification of LC3-II and LC3-II/I ratio, and SQSTM1/p62 levels after normalization with the expression of the loading control, β-actin, in cells with and without pretreatment with 20 nM bafilomycin A1. Data (mean ± SD); $n = 6$ (EFV10, EFV25), 7 (CCCP10) and 8 (for the rest) are expressed as % of the control (untreated cells, considered 100%). **(F)** Analysis of the mRNA levels of *ULK1, BECN-1* and *GABARAPL1* by quantitative RT-PCR. Data show mean ± SD: for *ULK1* $n = 4$, except for TG2 ($n = 3$) and EFV10 ($n = 4$); for *BECN-1* $n = 4$, except for EFV10 ($n = 3$) and CCCP10 ($n = 5$); and for *GABARAPL1* $n = 4$ except for EFV10 and CCCP10 ($n = 3$) and TG 2 ($n = 3$). Values express mRNA content in relation to that of control (untreated cells, considered 1) after normalization with the housekeeping gene *ACTB* (β-actin). **(G)** Analysis of the lysosomal content by flow cytometry using LysoTracker Green. A representative cytogram (left) and quantification of the fluorescence (right, mean ± SD, $n = 3$, fluorescence detected in vehicle-treated cells was considered 100%) are shown. **(I)** Representative images of live cell confocal fluorescence microscopy (63× augmentation and images with an additional 2× digital zoom) where lysosomes were stained with 0.1 μM LysoTracker Green. Statistical analysis was performed by a Student's *t*-test vs vehicle ($^{*}P < 0.05$, $^{**}P < 0.01$ and $^{***}P < 0.005$) and $\#\#\#P < 0.005$ with bafilomycin A1 versus without it. (For interpretation of the references to color in this figure legend, the reader is referred to the Web version of this article.)

microscopy (Fig. 1B) while punctae were lacking in Rot-exposed cells in agreement with the data obtained by Western blot. Degradation of SQSTM1/p62 protein is widely recognized as an autophagy marker, as it directly binds to LC3 and is selectively degraded by autophagy (Klionsky et al., 2016). We observed this effect with CCCP, but the contrary was detected with EFV, TG and Rot. p62 accumulation can be a sign of blockage in the autophagic process, but may also be caused by other factors, including enhanced *SQSTM1* transcription and *de novo* protein synthesis, which seemed to be the case in EFV- and TG-treated cells, as revealed by qRT-PCR (Fig. 1C). We also studied the protein markers of autophagy in primary culture of rat astrocytes (Fig. 1D). Treatment (24 h) with EFV lead to an increase in both LC3 and p62 levels which underscores that the effect of EFV observed in U251-MG cells is not related to the cell line. Regarding CCCP, we did not detect an increase of LC3-II and also p62 was enhanced meaning that primary rat astrocytes may display somewhat different response to CCCP which may reflect greater susceptibility to this uncoupler. In order to assess autophagic flux, we determined lysosome-dependent degradation using bafilomycin A1. Analysis of the difference in the amount of LC3-II between samples with and without this lysosomal inhibitor revealed functional autophagic flux after treatment with both EFV and CCCP (Fig. 1E). Nevertheless, the increase in the LC3-II level in cells treated with EFV or CCCP in the presence of bafilomycin A1compared to vehicle is lower than that registered in absence of the lysosomal inhibitor which may indicate certain alteration in the autophagic flux, but given that this is observed with the control condition CCCP, it may be an effect related to the cell type/line. We also evaluated the mRNA levels of three crucial general autophagy mediators: ULK1, Beclin-1 and GABARAPL1. Atg1/ULK1 takes part in the initial steps of autophagy and has an important role in nutrient sensing and starvation-induced autophagy (Wong et al., 2013). Beclin1 is essential for nucleation (a specific step of autophagy), as part of Beclin 1-Vps34-Vps15 core complexes. GABARAPL1 promotes autophagic flux by enhancing the advanced stages of autophagy (Boyer-Guittaut et al., 2014). EFV enhanced mRNA levels of all three autophagic markers (Fig. 1F). Greater upregulation was observed in TG-treated cells, while, interestingly, either no changes or a significant decrease was detected with Rot. Lastly, we also studied lysosomes by flow cytometry, a widely accepted indicator of increased autophagy (Chikte et al., 2014), discovering that EFV, TG and CCCP enhanced LysoTracker fluorescence while Rot failed to do so (Fig. 1G). This was also observed with live-cell fluorescence microscopy imaging (Fig. 1I) which enabled us to explore lysosomal morphology detecting differences between EFV- and CCCP. With CCCP the signal was intense but dotted while EFV-treated cells exhibited big, round spheres indicative of large and fused lysosomal particles. Considered together, these results point to an increased volume of autophagosomes and lysosomes in EFV-treated cells, which has been described as an indicator of activated autophagy. In order to analyze the specificity of the effect observed in EFV in relation to other antiretroviral drugs, we treated U251-MG cells (24 h) with clinically relevant concentrations of two other widely employed anti-HIV drugs, representatives of the NRTI (abacavir, ABC) and NNRTI (rilpivirine, RPV) families. As shown in Fig. 2, neither ABC nor RPV induce significant changes in the protein levels of LC3 and p62, pointing to the fact that action of EFV is drug-specific.

3.2. EFV fails to activate canonical (CCCP-like) mitophagy

3.2.1. Analysis of mitochondrial markers of mitophagy

Next, we explored whether EFV-treated cells also display augmented mitophagy. We evaluated PINK1 and Parkin, mediators of PINK1/Parkin-dependent mitophagy, but found no increase with EFV (Fig. 3A); in fact, a decrease was observed in the mRNA levels of both markers with EFV25. TG enhanced mRNA of both *PINK1* and *Parkin* (Fig. 3B), an effect that was absent at protein level (Fig. 3A). Lastly, we addressed the mRNA level of the OMM protein BNIP3 and its homolog NIX/BNIP3L. Nix is not only required for CCCP-induced Parkin recruitment, but is also involved in the recruitment of the autophagic machinery to the damaged mitochondria by directly interacting with LC3 and GABARAP (Novak et al., 2010). While CCCP significantly enhanced both mRNA levels, EFV either provoked no changes (*BNIP3*) or cause a decrease (*NIX*). Of note, nearly all the markers decreased in Rot-treated cells. In conclusion, EFV does not seem to enhance classical mitophagy-related proteins.

3.2.2. Analysis of mitochondrial protein expression and mitochondrial mass

The assessment of mitochondrial protein expression and mass has been accepted as a measure of degradation of mitochondria and, hence, activation of mitophagy. We determined mitochondrial mass by flow cytometry using the fluorochrome MitoTracker Green, which reacts with free thiol groups of cysteine residues, thus covalently binding mitochondrial proteins, therefore unlike with tetramethylrhodamine methyl ester (TMRM) and other mitochondrial dyes, staining is not lost when there is a drop in $\Delta\Psi_m$. As expected, CCCP led to diminished mitochondrial mass, while an increase in the signal was detected with EFV (Fig. 4A). The evaluation of mitochondrial mass as well as morphology was also performed with live cell fluorescence microscopy in which mitochondria were labelled with MitoTracker Red (Fig. 4B). While we observed a decrease in the overall mitochondrial mass with CCCP, this was not evident with EFV. Moreover, mitochondria in EFV-treated cells displayed altered morphology (loss of the mitochondrial network) and altered localization/distribution (arranged in the

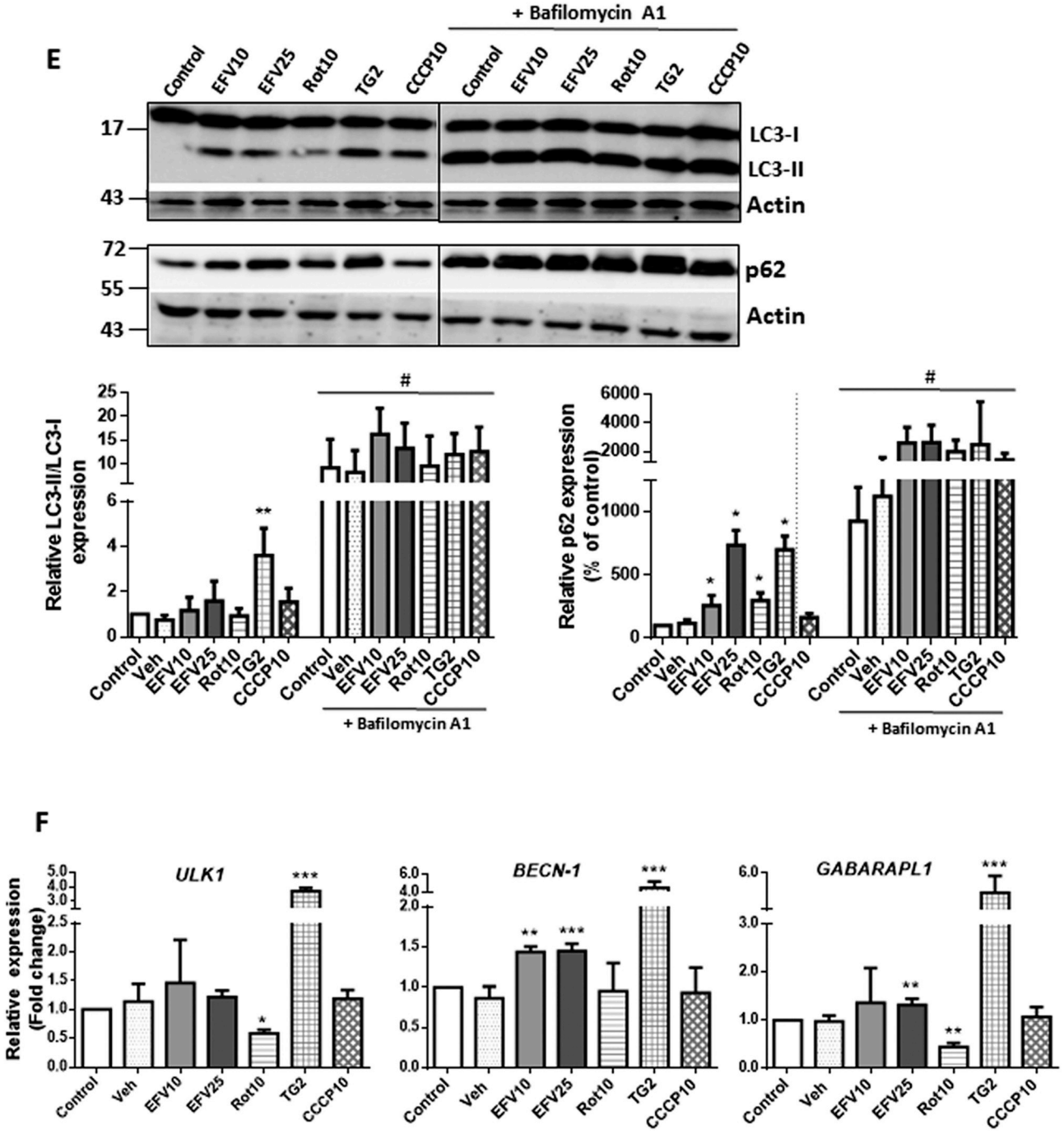

Fig. 1. (*continued*)

perinuclear area). Given that mitophagy can be quantified by decreased expression of mitochondrial proteins, and bearing in mind that Parkin can also mediate proteasome-dependent degradation of OMM proteins, we evaluated the expression, not only of OMM proteins such as voltage-dependent anion channel-1 (VDAC1) and translocase of the outer membrane-20 (TOM20), but also of mitochondrial matrix protein representatives aconitase 2 (ACO2), ATP-dependent Clp protease ATP-binding subunit clpX-like (CLPX) and mitochondrial trifunctional enzyme subunit alpha (HADHA). While CCCP reduced the levels of VDAC1, CLPX and HADHA (and not of ACO2), EFV only diminished those of TOM20, and even significantly incremented the expression of VDAC1 (Fig. 4C). No significant alterations were observed with Rot, whereas TG slightly reduced CLPX and HADHA expression. In order to better understand the effect of EFV on the TOM20 and VDAC1 protein levels, we also assessed their mRNA by qRT-PCR, discovering that the drug did not alter *TOMM20* expression (Fig. 4D), thus proving that the decreased TOM20 content was not due to reduced gene transcription. On the contrary, EFV led to a slight increase in *VDAC1* mRNA levels, an effect that correlated with (and could be the reason for) the increased VDAC1 protein expression. In conclusion, EFV fails to induce general mitochondrial degradation (classical mitophagy) and alternatively may mediate a different degradation as seen by the decrease in the protein content of TOM20.

3.2.3. Analysis of mitochondrial colocalization with autophagosomes and lysosomes

Next, we performed confocal fluorescence microscopy experiments in order to assess the colocalization of mitochondria and

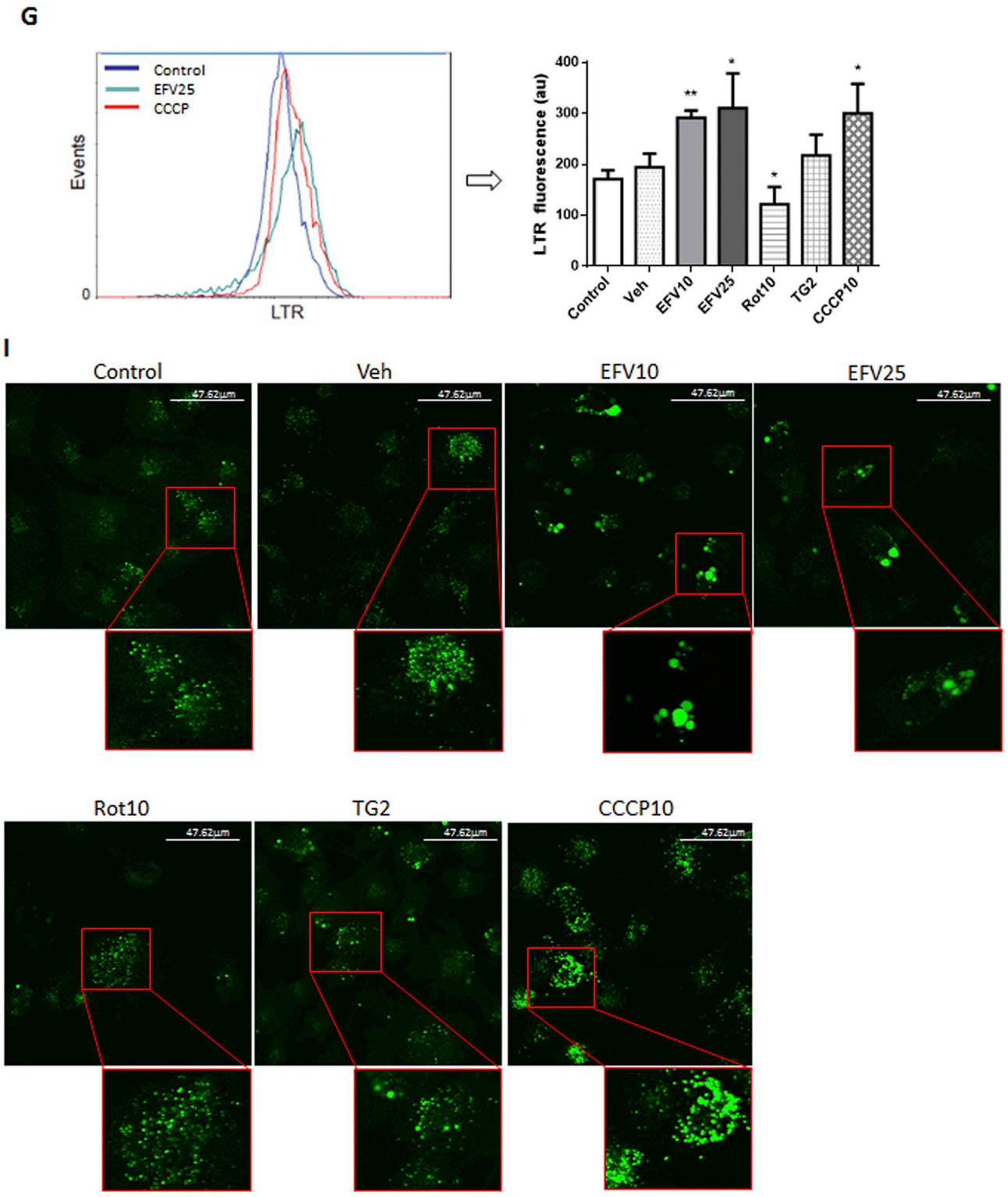

Fig. 1. (*continued*)

autophagosomes. An immunocytochemistry approach was employed using TOM20 as a mitochondrial marker and LC3 to label autophagosomes. The images reflect the changes in the mitochondrial morphology produced by all the treatments (loss of the mitochondrial network) and the dramatic increase in LC3 staining with EFV and TG (Fig. 5A). Moreover, colocalization analysis revealed increased overlapping of the mitochondrial signal with autophagosomes in EFV- or TG-exposed cells (Fig. 5A). In the case of CCCP, increased colocalization was observed only in the perinuclear area. Perinuclear aggregation of depolarized mitochondria (sometimes in the form of large perinuclear clusters) is considered a hallmark of mitophagy (Vives-Bauza et al., 2010). A more in-depth analysis of the images with overlapped signals from mitochondria (TOM20) and autophagosomes (LC3) revealed spatial differences between EFV- and CCCP-treated cells (Fig. 5B). As expected, in cells exposed to the vehicle, there was little colocalization; on the contrary, intense superposing was induced by both EFV and CCCP.

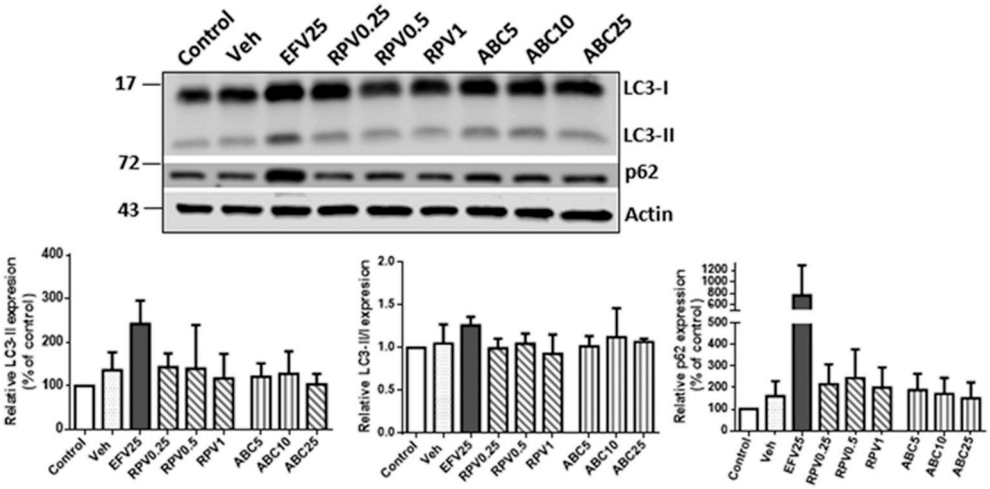

Fig. 2. Analysis of autophagy markers after treatment with other antiretroviral drugs. U251-MG cells were treated with vehicle (DMSO), EFV (25 μM), RPV (0.25, 0.5 and 1 μM) or ABC (5, 10 and 25 μM) for 24 h. Immunoblot analysis showing representative Western blotting images and histograms expressing quantification of LC3-II, LC3II/I ratio and p62 levels after normalization with the expression of the loading control, β-actin. Data (mean ± SD, $n = 3$) are expressed as % of control (untreated cells, considered 100%).

However, while in CCCP-treated cells this colocalization was evident in the mitochondria aggregated in the perinuclear region, in EFV-treated cells, the area adjacent to the nucleus contained LC3 but no TOM20-positive mitochondria. To explore further the mechanisms of mitochondrial clearance induced by EFV, we aimed to discriminate between healthy and depolarized mitochondria. To this end, we performed double staining confocal fluorescence microscopy in which cells were immunostained for p62 and labelled with Mitoview, a fluorescent $\Delta\Psi_m$–sensitive mitochondrial probe, revealing several interesting results. Firstly, cells treated with EFV25 displayed a severely damaged mitochondrial network (Fig. 5C). Despite the fact that these mitochondria maintained at least a substantial part of their $\Delta\Psi_m$, they formed unusual ring-like structures. The fact that this difference was not observed when a general mitochondrial marker was employed (TOM20) points to the presence of a large portion of depolarized mitochondria in EFV-treated cells. This is in agreement with our previous

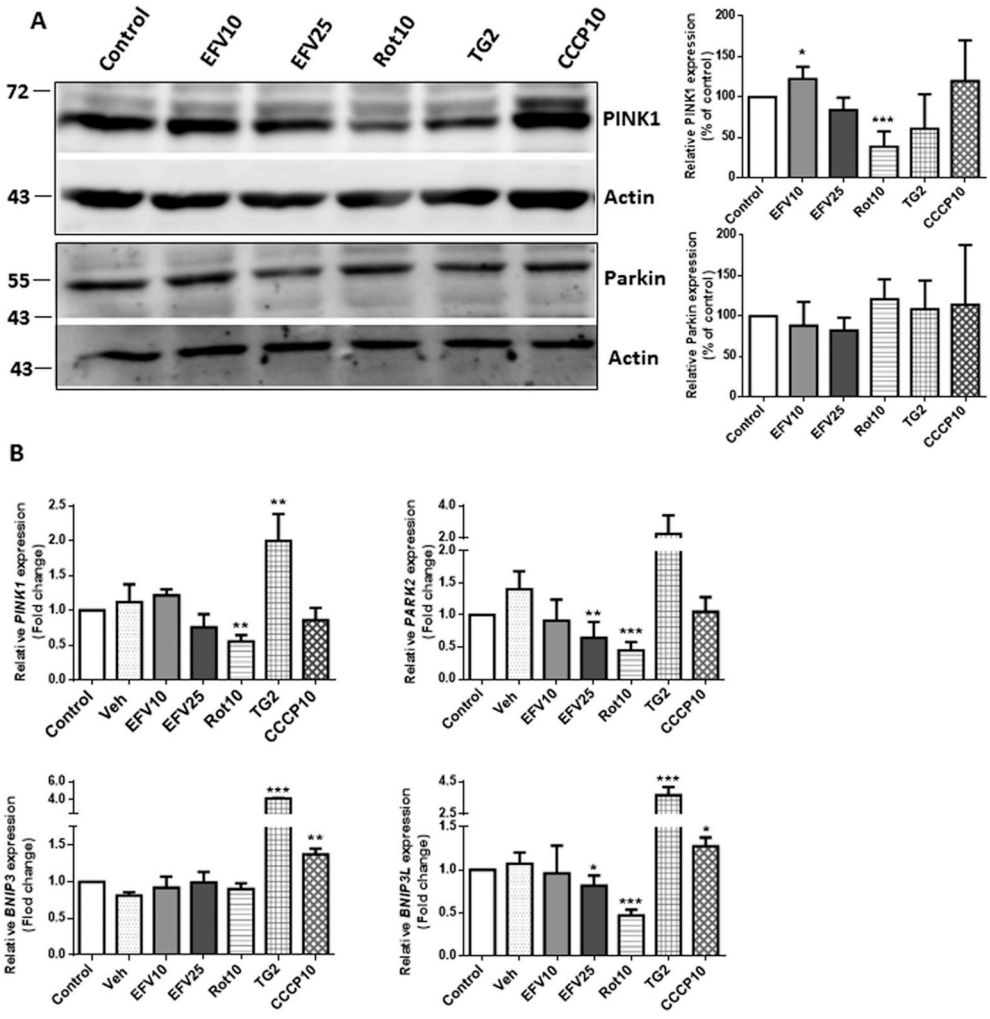

Fig. 3. Analysis of mRNA levels and protein expression of mitophagy markers. Cells were treated for 24 h with efavirenz (EFV10 and 25μ), vehicle (DMSO), thapsigargin (TG 2 μM), rotenone (Rot 25 μM) or CCCP 10 μM. **(A)** Immunoblot analysis showing a representative Western blotting image and histograms expressing quantification of PINK1 and Parkin levels after normalization with the expression of the loading control, β-actin. Data (mean ± SD, $n = 4$ for PINK1 except for CCCP10 $n = 3$, and $n = 4$ for Parkin) are expressed as % of control (untreated cells, considered 100%). **(B)** Analysis of the mRNA levels of *PINK1, PARK2, BNIP3* and *BNIP3L* by quantitative RT-PCR. Data, shown as mean ± SD; for *PINK1*, $n = 4$ (Veh, EFV10, EFV25 and TG2) and $n = 5$ (for the rest); for *PARK2*, $n = 5$ except for Veh ($n = 3$) and EFV10 ($n = 4$); for *BNIP3* $n = 4$ except for EFV10 and CCCP10 ($n = 3$); and for *BNIP3L*, $n = 4$. Values express mRNA content in relation to that of control (untreated cells, considered 1) after normalization with the housekeeping gene *ACTB* (β-actin). Statistical analysis was performed by Student's *t*-test vs control or vehicle ($^{*}P < 0.05$, $^{**}P < 0.01$ and $^{***}P < 0.005$).

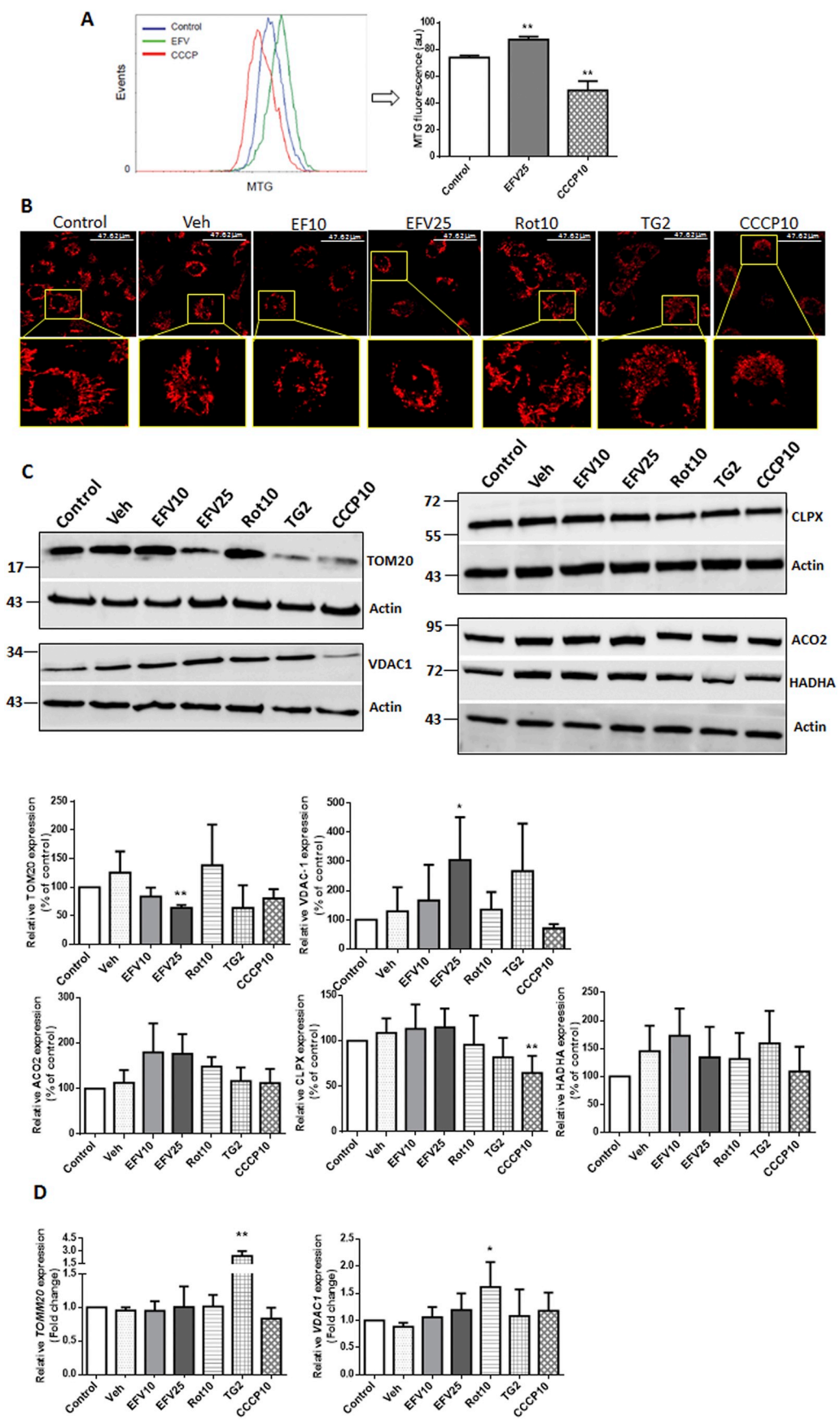

Fig. 4. Evaluation of mitochondrial mass and mitochondrial protein expression. Cells were treated for 24 h with efavirenz (EFV10 and 25 μM), vehicle (DMSO), thapsigargin (TG 2 μM), rotenone (Rot 25 μM) or CCCP 10 μM. **(A)** Analysis of the mitochondrial content by flow cytometry using MitoTracker Green (MTG). A representative cytogram (left) and quantification of the fluorescence (right, mean ± SD, $n = 3$, fluorescence detected in vehicle-treated cells was considered 100%) are shown. **(B)** Representative images of live cell-fluorescence microscopy (63× augmentation and images with an additional 4× digital zoom) where mitochondria were stained with 1 μM MitoTracker Red. **(C)** Immunoblot analysis showing a representative Western blotting image and histograms expressing quantification of TOM20, VDAC1, ACO2, CLPX and HADHA levels after normalization with the expression of the loading control, β-actin. Data show mean ± SD, for TOM20 $n = 4$ except for CCCP10 ($n = 3$); for VDAC1 $n = 5$ except for EFV25 and CCCP10 $n = 4$; for ACO2 $n = 3$ (Veh, EFV10, Rot10 and TG2) and $n = 4$ (for the rest); for CLPX $n = 5$ (Veh, EFV25, TG2 and CCCP10) or $n = 6$ (for the rest); and for HADHA $n = 5$ except for TG2 ($n = 4$). Values are expressed as % of control (untreated cells, considered 100%). **(D)** Analysis of the mRNA levels of *TOMM20* and *VDAC1* by quantitative RT-PCR. Data show as mean ± SD of *TOMM20,* $n = 5$ except for Veh, EFV10 and Rot10 ($n = 4$); and for *VDAC1,* $n = 4$ (Veh, EFV25, Rot10 and CCCP10) or $n = 5$ (for the rest). Values express mRNA content in relation to that of control (untreated cells, considered 1) after normalization with the housekeeping gene *ACTB* (β-actin). Statistical analysis was performed by Student's *t*-test vs control or vehicle ($^{*}P < 0.05$, $^{**}P < 0.01$ and $^{***}P < 0.005$). (For interpretation of the references to color in this figure legend, the reader is referred to the Web version of this article.)

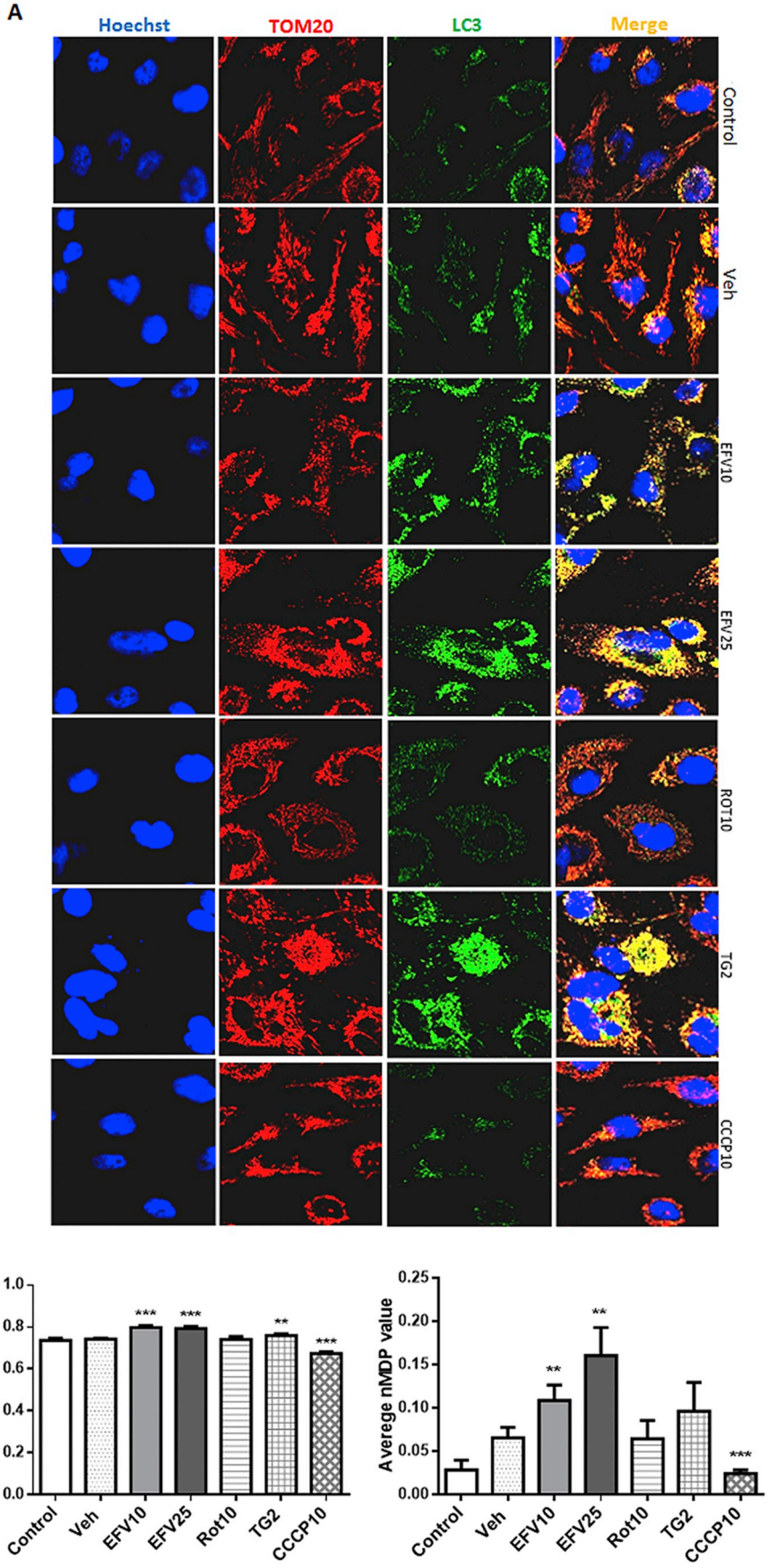

(caption on next page)

Fig. 5. Assessment of autophagosomes (LC3), mitochondria (TOM20) and presence of p62 by confocal fluorescence microscopy. Cells were treated for 24 h with efavirenz (EFV10 and 25μM), vehicle (DMSO), thapsigargin (TG 2 μM), rotenone (Rot 25 μM) or CCCP 10 μM. (**A**) Representative confocal fluorescence microscopy images (63 ×) of cells labelled with Hoechst 33342 (nuclei), anti-TOM20 (mitochondria) and anti-LC3 (autophagosomes). Colocalization was quantified by two means: histogram showing the index of correlation (I_{corr}) between the two signals (left) and the correlation between individual pairs of pixels (normalized mean deviation product-nMDP) (right), (mean ± SD, $n = 3$). (**B**) Representative confocal fluorescence microscopy images (63× plus 2× digital zoom) of cells labelled with Hoechst 33342 (nuclei), anti-TOM20 (mitochondria) and anti-LC3 (autophagosomes). **(C)** Assessment of p62 and mitochondria (TOM20) colocalization. Representative confocal fluorescence microscopy images (63 ×) of cells labelled with Hoechst 33342 (nuclei), Mitoview (mitochondria) and anti-p62 (autophagosomes). Colocalization was quantified by two means: histogram showing the index of correlation (I_{corr}) between the two signals (left) and deviation product-nMDP (right), (mean ± SD, $n = 3$).

studies which have shown that 24 h-treatment with EFV (10 and 25 μM) lead to a major drop in $\Delta\Psi_m$ in both U251-MG cells and primary astrocytes, comparable to the effect exhibited by the mitochondrial uncoupler FCCP (Funes et al., 2014). Moreover, unlike the rest of the treatments, EFV25-exposed cells exhibited – somewhat unexpectedly - a significant degree of overlapping between the mitochondrial signal (red, Mitoview) and the immunofluorescence originated by p62 (green), as shown in Fig. 5C.

Considered together, these data point to the absence of classical mitophagy in EFV-treated cells, while suggesting the existence of an alternative way of mitochondrial degradation.

4. Discussion

Mitochondria are double-membrane organelles present in eukaryotic cells that fulfill central roles in energy metabolism, synthesis of

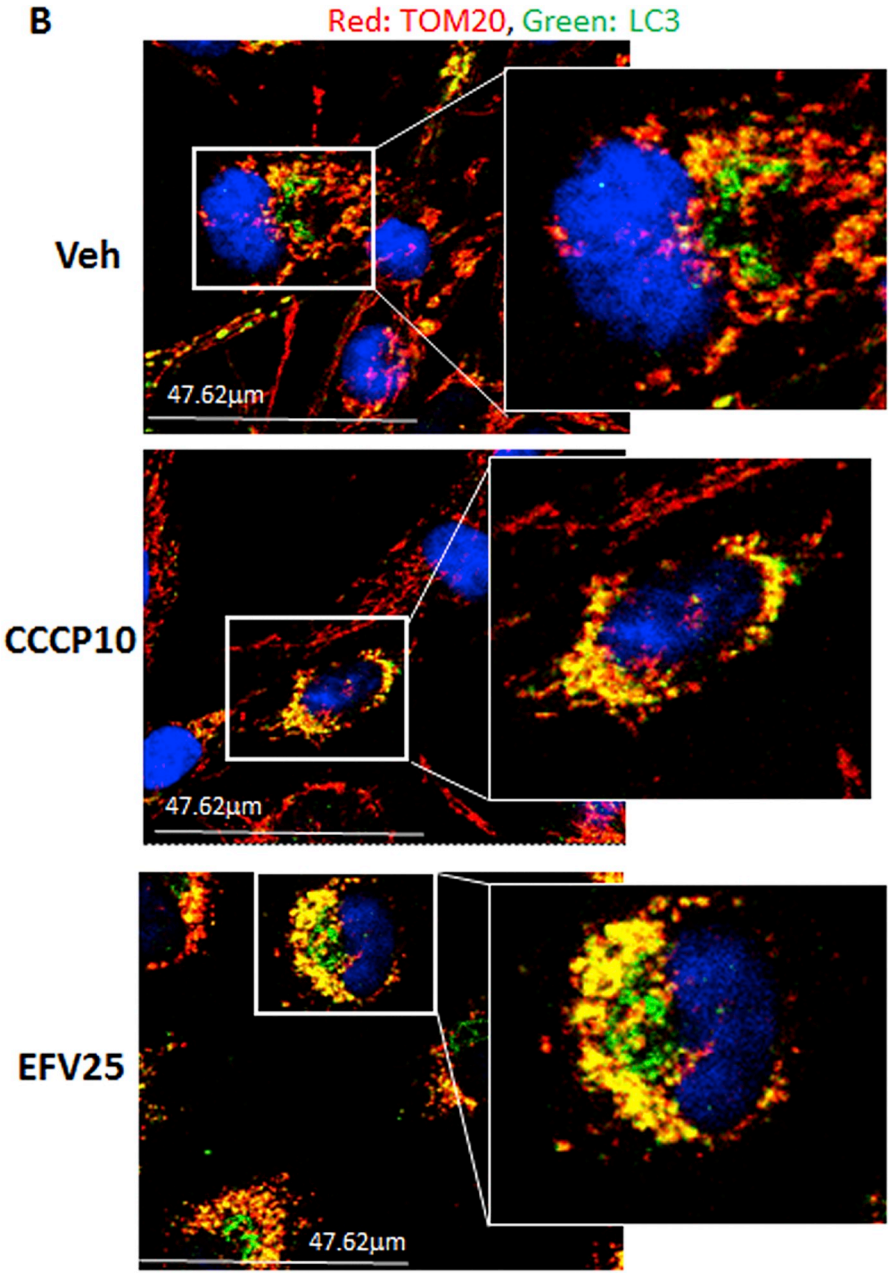

Fig. 5. (*continued*)

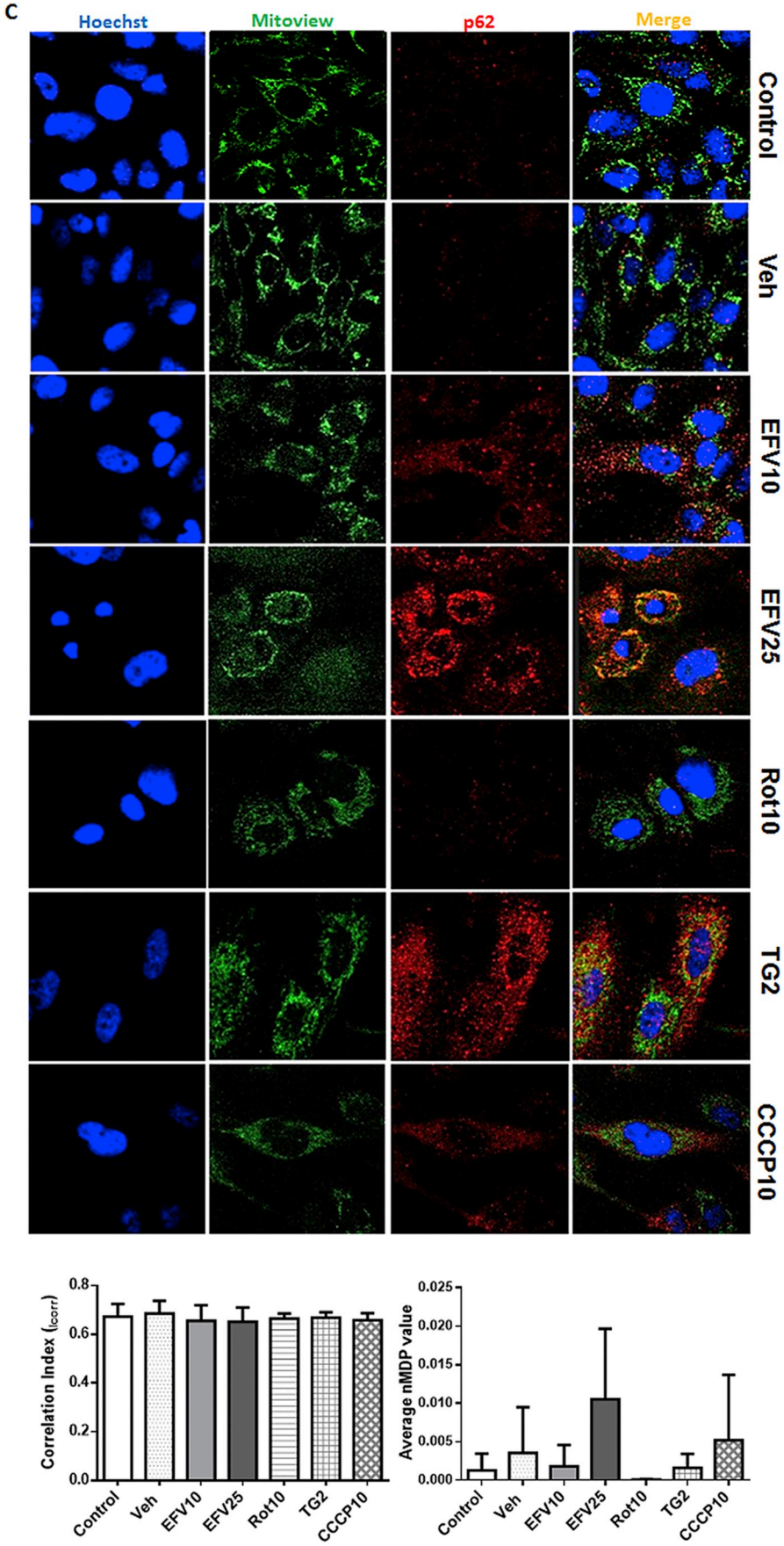

Fig. 5. (*continued*)

amino acids, lipids and Fe–S clusters, ion homeostasis, thermogenesis and regulation of cell death. Mitochondrial dysfunction is closely linked to numerous chronic diseases, including neurodegenerative disorders and aging (Grimm and Eckert, 2017), and drug-induced neurotoxicity (Mark and Don, 2007). Multiple studies have provided evidence that EFV interferes with mitochondrial function in the brain, thus constituting a mechanism that may participate in EFV-related CNS side effects, alterations of major clinical relevance in the pharmacological treatment of HIV infection. Mitochondrial quality control is an essential process that occurs on many levels. On the organellar level, dysfunctional/damaged mitochondria are detected, engulfed by autophagosomes and cleared by a selective type of autophagy called mitophagy (Lyamzaev et al., 2004; Kim et al., 2007). Depolarization seems to be a consistent feature in mammalian mitophagy (Tolkovsky, 2009), and mitophagy is typically induced in cultured cells by the mitochondrial uncoupler CCCP. Nevertheless, the use of uncouplers as a mitophagy model is not ideal, as the entire mitochondrial network becomes depolarized, which is not expected to occur in real-life situations. Mitochondrial membrane depolarization initiates PINK1-mediated mitophagy, the best understood mechanism of mitophagy; however, additional mechanisms, other than or independent of mitochondrial depolarization, are involved in PINK1 accumulation, such as the presence of mitochondrial DNA (mtDNA) mutations or the excessive amount of unfolded proteins in the mitochondrial matrix (King et al., 2017).

Mitochondria represent a major physiological source of ROS, molecules which cause oxidative damage to virtually all cellular components but which also serve as important signaling molecules for the induction of autophagy (Scherz-Shouval and Elazar, 2011; Lee et al., 2012). They have been attributed multiple actions, including ROS-caused inhibition of the mTOR signaling pathway, a major mediator of autophagy, and inactivation of Atg4 which reduces its de-conjugation activity thus increasing LC3 association with the autophagosomal membrane (Scherz-Shouval et al., 2007). Accumulated evidence pinpoints mitochondrial ROS generation (also a consequence of membrane depolarization) as an important mediating factor in the activation of mitophagy; however, the mechanisms at play remain unclear, as when mitophagy was induced by ROS, it simultaneously involved the induction of non-selective autophagy in virtually all cases. Rot, an inducer of mitochondrial superoxide has been shown to induce mitophagy in neurons (PC12 cells differentiated into neuron-like cells) (Peng et al., 2019). In the present model, Rot failed to upregulate mitophagy, which may be because major oxidative stress can inhibit mitophagy by modification and inactivation of Parkin. Parkin contains multiple conserved cysteine residues that are important for maintaining its solubility (Wong et al., 2007), but which are also susceptible to modification by oxidative and nitrosative stress, leading to the inactivation and aggregation of Parkin (Winklhofer et al., 2003; Chung et al., 2004). In U251-MG cells and primary rat astrocytes, EFV interferes with the mitochondrial ETC by inhibiting Complex I and to a lesser extent Complex IV, and enhances mitochondrial ROS generation (Funes et al., 2014; Apostolova et al., 2015a,b). Despite certain similarities between their mitochondrial actions, in the present work, EFV and Rot produce quite a different response, possibly related to the difference in their primary effect-while Rot acts as a stronger Complex I inhibitor and superoxide generator, EFV has the capacity to also produce ER stress. Given this latter fact, we also compared its effects with those of TG, a bona fide ER stressor that has been shown to induce Parkin-2 dependent mitophagy in both primary murine cortical neurons and a mouse model of ischemia-reperfusion-induced brain injury (Zhang et al., 2014). In our hands, TG induced autophagy but did not seem to induce classic mitophagy.

In the present study, we have assessed the capacity of EFV to induce autophagy/mitophagy in a previously described model of EFV-treated human glioblastoma cells. We present evidence of induction of autophagy and the presence of functional autophagic flux, despite the accumulation of p62. The role of p62 in mitophagy is controversial; while it is recruited to damaged mitochondria (Ding et al., 2010; Geisler et al., 2010), p62/SQSTM1 null cells have no defect in Parkin-mediated mitophagy, and p62 is not essential for mitophagic degradation of mitochondria (Ding et al., 2010; DP Narendra et al., 2010; Okatsu et al., 2010; Strappazzon et al., 2015). Alternatively, it controls mitochondrial distribution and, for that matter, Parkin-induced mitochondrial clustering (D Narendra et al., 2010). Our result that mitochondria colocalize with p62 in EFV-exposed cells is particularly interesting. p62 is a multifunctional protein that not only participates in autophagy and offers protection against oxidative stress but has also been attributed a direct role in maintaining functional mitochondrial energetics and mtDNA stability. This role has been associated with its localization at mitochondria and deficiency in p62 exacerbates defects in $\Delta\Psi_m$ and energetics leading to mitochondrial dysfunction (Seibenhener et al., 2013).

The evidence we present points to lack of canonical mitophagy in EFV-treated cells. In contrast to the classic mitophagy inducer CCCP, mitochondrial mass did not decrease and there was no up-regulation in the mRNA levels of mitophagy genes. Nevertheless, we detected increased colocalization between TOM20 and autophagosomes, accompanied by a decrease in TOM20 levels, suggesting that this protein was effectively degraded. According to current knowledge in this field, mitophagy is no longer viewed as an “all or nothing“ phenomenon, and damaged parts of mitochondria can be removed while other portions persist. In addition, mitochondria can hyperfuse, a mechanism that counteracts mitochondrial degradation upon starvation, when ROS levels are high and non-selective forms of autophagy are induced (Frank et al., 2012). Mitophagy can be quantified by decreased mitochondrial protein content; however, other simultaneously occurring processes, including proteasomal degradation and altered biogenesis, leading to under- or overestimation of mitophagy can heavily influence such changes. In this vein, early studies of mitophagy used degradation of the OMM protein TOM20 as a marker of mitochondrial mass. However, Parkin also mediates proteasome-dependent degradation of OMM proteins including TOM20 (Yoshii et al., 2011), in addition to mitophagy; therefore, loss of OMM proteins alone is not a sufficient measure. Another line of mitochondrial defense against damage involves mitochondrial-derived vesicles (MDVs) (Soubannier et al., 2012) which grow from mitochondria and deliver sequestered cargo to lysosomes for degradation. This pathway, active under steady-state conditions and further activated by oxidative stress, involves both PINK1 and Parkin, and is different from canonical mitophagy (Sugiura et al., 2014). We cannot rule out that this process is active in our model, and future studies should seek to confirm it.

Of note, during mitophagy, damaged mitochondria form a perinuclear cluster, which is subsequently eliminated. While we could clearly observe such relocation of mitochondria in EFV-treated cells, it differed from that detected in CCCP-exposed cells. After EFV treatment, a significant area subjacent to the nucleus contained autophagosomes but was TOM20-free; this may be because, besides being a crucial player in mitochondrial protein import, TOM20 has also been attributed a role in perinuclear aggregation of mitochondria (Yano et al., 1997). We can speculate that the specific degradation of TOM20 in EFV-exposed cells impairs perinuclear mitochondrial aggregation in a way that facilitates their mitophagic clearance. Importantly, other studies have also provided evidence of TOM20-negative mitochondria, as in the case of CCCP-treated Parkin overexpressing HeLa and SHSY-5Y cells, a phenomenon attributed to degradation of TOM20 by the proteasome preceding mitophagy (Chan et al., 2011).

Collectively, our findings demonstrate that EFV triggers autophagy, but does not induce canonical mitophagy in U251-MG cells. We cannot rule out the possibility that other forms of mitophagy exist and are independent of ubiquitin labeling, PINK1/Parkin function and cytosolic receptors. Indeed, the results presented here support the existence of an alternative mitochondrial degradation that does not lead to massive

clearance and may involve only partial removal of parts of these organelles. Nevertheless, whether alternative mechanisms of mitophagy are present in this model and which mechanisms govern them is an issue that needs to be explored in future studies. Another obvious limitation of the present work is its *in vitro* setting, and whether or not the findings displayed here occur *in vivo* is unknown at present. Moreover, in some parameters, the effect exerted by EFV is not concentration-dependent. In summary, the effect described herein may help to better understand the mechanisms of EFV-related CNS side effects, specifically regarding EFV-induced mitochondrial alterations in astrocytes, and thus may have potential clinical relevance for the better management of HIV patients and in particular regarding the development of HAND.

Disclosure statement

J.V.E. has received funds for speaking at symposia organized by Abbvie Farmacéutica S.L.U., Astra Zeneca and Gilead Sciences. Other authors: none to declare.

Author contributions

OM-A, AG, VM-V, SMSY-D and RAG-P performed experiments and analyzed data; AB-G, JMF, JVE and NA designed experiments, prepared the figures, critically revised data; NA and AB-G drafted and wrote the MS.

Funding and acknowledgements

This work was funded by the Instituto de Salud Carlos III, Ministerio de Economía, Industria y Competitividad (research grants PI14/00312, PI15/00034, CIBER CB06/04/0071 and CIBERNED CB06/05/004) and the Conselleria d'Educació, Formació i Ocupació, Generalitat Valenciana (research grant GVA/2014/118) and was also partially supported by "Fondo Europeo de Desarrollo Regional" (FEDER) from the European Union. SMSY-D was supported by Isabel Gemio Foundation. RAG-P is the recipient of a "Contrato destinado a la retención y atracción del talento investigador, TA13009" from Junta de Extremadura and AG is supported by the Foundation "Juan Esplugues". We would also like to acknowledge the support of the TRANSAUTOPHAGY COST Action, CA15138.

The authors thank Brian Normanly for his English language editing.

Appendix A. Supplementary data

Supplementary data to this article can be found online at https://doi.org/10.1016/j.antiviral.2019.04.015.

References

Abers, M.S., Shandera, W.X., Kass, J.S., 2014. Neurological and psychiatric adverse effects of antiretroviral drugs. CNS Drugs 28 (2), 131–145.
Apostolova, N., Gomez-Sucerquia, L.J., Gortat, A., et al., 2011. Compromising mitochondrial function with the antiretroviral drug efavirenz induces cell survival-promoting autophagy. Hepatology 54 (3), 1009–1019.
Apostolova, N., Funes, H.A., Blas-Garcia, A., et al., 2015a. Efavirenz and the CNS: what we already know and questions that need to be answered. J. Antimicrob. Chemother. 70 (10), 2693–2708.
Apostolova, N., Funes, H.A., Blas-Garcia, A., Alegre, F., Polo, M., Esplugues, J.V., 2015b. Involvement of nitric oxide in the mitochondrial action of efavirenz: a differential effect on neurons and glial cells. J. Infect. Dis. 211 (12), 1953–1958.
Arendt, C., Rother, A., Stolte, S., Dringen, R., 2016. Consequences of a chronic exposure of cultured brain astrocytes to the anti-retroviral drug efavirenz and its primary metabolite 8-hydroxy efavirenz. Neurochem. Res. 41 (12), 3278–3288.
Boyer-Guittaut, M., Poillet, L., Liang, Q., et al., 2014. The role of GABARAPL1/GEC1 in autophagic flux and mitochondrial quality control in MDA-MB-436 breast cancer cells. Autophagy 10 (6), 986–1003.
Carr, A., Cooper, D.A., 2000. Adverse effects of antiretroviral therapy. Lancet 356 (9239), 1423–1430.
Chan, N.C., Salazar, A.M., Pham, A.H., et al., 2011. Broad activation of the ubiquitin-proteasome system by Parkin is critical for mitophagy. Hum. Mol. Genet. 20 (9), 1726–1737.
Chikte, S., Panchal, N., Warnes, G., 2014. Use of LysoTracker dyes: a flow cytometric study of autophagy. Cytometry 85 (2), 169–178.
Choi, A.M., Ryter, S.W., Levine, B., 2013. Autophagy in human health and disease. N. Engl. J. Med. 368 (7), 651–662.
Chung, K.K., Thomas, B., Li, X., et al., 2004. S-nitrosylation of parkin regulates ubiquitination and compromises parkin's protective function. Science 304 (5675), 1328–1331.
Clifford, D.B., Ances, B.M., 2013. HIV-associated neurocognitive disorder. Lancet Infect. Dis. 13 (11), 976–986.
Davis, C.H., Kim, K.Y., Bushong, E.A., et al., 2014. Transcellular degradation of axonal mitochondria. Proc. Natl. Acad. Sci. U. S. A. 111 (26), 9633–9638.
Ding, W.X., Ni, H.M., Li, M., et al., 2010. Nix is critical to two distinct phases of mitophagy, reactive oxygen species-mediated autophagy induction and Parkin-ubiquitin-p62-mediated mitochondrial priming. J. Biol. Chem. 285 (36), 27879–27890.
Dong, Q., Oh, J.E., Yi, J.K., et al., 2013. Efavirenz induces autophagy and aberrant differentiation in normal human keratinocytes. Int. J. Mol. Med. 31 (6), 1305–1312.
Frank, M., Duvezin-Caubet, S., Koob, S., et al., 2012. Mitophagy is triggered by mild oxidative stress in a mitochondrial fission dependent manner. Biochim. Biophys. Acta 1823 (12), 2297–2310.
Funes, H.A., Apostolova, N., Alegre, F., et al., 2014. Neuronal bioenergetics and acute mitochondrial dysfunction: a clue to understanding the central nervous system side effects of efavirenz. JID (J. Infect. Dis.) 210 (9), 1385–1395.
Geisler, S., Holmström, K.M., Skujat, D., et al., 2010. PINK1/Parkin-mediated mitophagy is dependent on VDAC1 and p62/SQSTM1. Nat. Cell Biol. 12 (2), 119–131.
Grimm, A., Eckert, A., 2017. Brain aging and neurodegeneration: from a mitochondrial point of view. J. Neurochem. 143 (4), 418–431.
Jaskolski, F., Mulle, C., Manzoni, O.J., 2005. An automated method to quantify and visualize colocalized fluorescent signals. J. Neurosci. Methods 146 (1), 42–49.
Jiang, P., Mizushima, N., 2015. LC3- and p62-based biochemical methods for the analysis of autophagy progression in mammalian cells. Methods 75, 13–18.
Kim, I., Rodriguez-Enriquez, S., Lemasters, J.J., 2007. Selective degradation of mitochondria by mitophagy. Arch. Biochem. Biophys. 462 (2), 245–253.
King, L., Plun-Favreau, H., 2017. Mitophagy. In: Verstreken, P. (Ed.), P*arkinson's Disease: Molecular Mechanisms Underlying Pathology*. Elsevier978-0-12-803783-6, .
Klionsky, D.J., et al., 2016. Guidelines for the use and interpretation of assays for monitoring autophagy (3rd ed.). Autophagy 12 (1), 1–222.
Lee, J., Giordano, S., Zhang, J., 2012. Autophagy, mitochondria and oxidative stress: cross-talk and redox signalling. Biochem. J. 441, 523–540.
Lyamzaev, K.G., Pletjushkina, O.Y., Saprunova, V.B., et al., 2004. Selective elimination of mitochondria from living cells induced by inhibitors of bioenergetic functions. Biochem. Soc. Trans. 32 (Pt 6), 1070–1071.
Ma, Q., Vaida, F., Wong, J., et al., 2016. Long-term efavirenz use is associated with worse neurocognitive functioning in HIV-infected patients. J. Neurovirol. 22 (2), 170–178.
Magistretti, P.J., Allaman, I., 2018. Lactate in the brain: from metabolic end-product to signalling molecule. Nat. Rev. Neurosci. 19 (4), 235–249.
Mark, R.B., Don, J.M., 2007. Drug-induced disorders of the nervous system. Clin. Med. 7 (2), 170–176.
Narendra, D.P., Jin, S.M., Tanaka, A., et al., 2010. PINK1 is selectively stabilized on impaired mitochondria to activate Parkin. PLoS Biol. 8 (1), e1000298.
Narendra, D., Kane, L.A., Hauser, D.N., et al., 2010. p62/SQSTM1 is required for Parkin-induced mitochondrial clustering but not mitophagy; VDAC1 is dispensable for both. Autophagy 6 (8), 1090–1106.
Novak, I., Kirkin, V., McEwan, D.G., et al., 2010. Nix is a selective autophagy receptor for mitochondrial clearance. EMBO Rep. 11 (1), 45–51.
Ojeda, D.S., Grasso, D., Urquiza, J., Till, A., Vaccaro, M.I., Quarleri, J., 2018. Cell death is counteracted by mitophagy in HIV-productively infected astrocytes but is promoted by inflammasome activation among non-productively infected cells. Front. Immunol. 9, 2633.
Okatsu, K., Saisho, K., Shimanuki, M., et al., 2010. p62/SQSTM1 cooperates with Parkin for perinuclear clustering of depolarized mitochondria. Genes Cells 15 (8), 887–900.
Peng, K., Xiao, J., Yang, L., et al., 2019. Mutual antagonism of PINK1/parkin and PGC-1α contributes to maintenance of mitochondrial homeostasis in rotenone-induced neurotoxicity. Neurotox. Res. 35 (2), 331–343.
Purnell, P.R., Fox, H.S., 2014. Efavirenz induces neuronal autophagy and mitochondrial alterations. J. Pharmacol. Exp. Ther. 351 (2), 250–258.
Scherz-Shouval, Elazar, Z., 2011. Regulation of autophagy by ROS: physiology and pathology. Trends Biochem. Sci. 36 (1), 30–38.
Scherz-Shouval, R., Shvets, E., Fass, E., et al., 2007. Reactive oxygen species are essential for autophagy and specifically regulate the activity of Atg4. EMBO J. 26 (7), 1749–1760.
Seibenhener, M.L., Du, Y., Diaz-Meco, M.T., et al., 2013. A role for sequestosome 1/p62 in mitochondrial dynamics, import and genome integrity. Biochim. Biophys. Acta 1833 (3), 452–459.
Shah, A., Gangwani, M.R., Chaudhari, N.S., et al., 2016. Neurotoxicity in the post-HAART era: caution for the antiretroviral therapeutics. Neurotox. Res. 30 (4), 677–697.
Shi, J., Fung, G., Deng, H., et al., 2015. NBR1 is dispensable for PARK2-mediated mitophagy regardless of the presence or absence of SQSTM1. Cell Death Dis. 6 (10), e1943.
Soubannier, V., McLelland, G.L., Zunino, R., et al., 2012. A vesicular transport pathway shuttles cargo from mitochondria to lysosomes. Curr. Biol. 22 (2), 135–141.
Strappazzon, F., Nazio, F., Corrado, M., et al., 2015. AMBRA1 is able to induce mitophagy via LC3 binding, regardless of PARKIN and p62/SQSTM1. Cell Death Differ. 22 (3), 419–432.
Streck, E.L., Ferreira, G.K., Scaini, G., et al., 2011. Non-nucleoside reverse transcriptase

inhibitors efavirenz and nevirapine inhibit cytochrome C oxidase in mouse brain regions. Neurochem. Res. 36 (6), 962–966.
Sugiura, A., McLelland, G.L., Fon, E.A., et al., 2014. A new pathway for mitochondrial quality control: mitochondrial-derived vesicles. EMBO J. 33 (19), 2142–2156.
Tolkovsky, A.M., 2009. Mitophagy. Biochim. Biophys. Acta 1793 (9), 1508–1515.
Ton, H., Xiong, H., 2013. Astrocyte dysfunctions and HIV-1 neurotoxicity. J. AIDS Clin. Res. 4 (11), 255.
Vives-Bauza, C., Zhou, C., Huang, Y., et al., 2010. PINK1-dependent recruitment of Parkin to mitochondria in mitophagy. Proc. Natl. Acad. Sci. U. S. A. 107 (1), 378–383.
Weiß, M., Kost, B., Renner-Müller, I., et al., 2016. Efavirenz causes oxidative stress, endoplasmic reticulum stress, and autophagy in endothelial cells. Cardiovasc. Toxicol. 16 (1), 90–99.
Winklhofer, K.F., Henn, I.H., Kay-Jackson, P.C., et al., 2003. Inactivation of parkin by oxidative stress and C-terminal truncations: a protective role of molecular chaperones. J. Biol. Chem. 278 (47), 47199–47208.
Wong, E.S., Tan, J.M., Wang, C., Zhang, Z., Tay, S.P., Zaiden, N., et al., 2007. Relative sensitivity of parkin and other cysteine-containing enzymes to stress-induced solubility alterations. J. Biol. Chem. 282 (16), 12310–12318.
Wong, P.-M., Puente, C., Ganley, I.G., et al., 2013. The ULK1 complex: sensing nutrient signals for autophagy activation. Autophagy 9 (2), 124–137.
Yamamoto, A., Tagawa, Y., Yoshimori, T., et al., 1998. Bafilomycin A1 prevents maturation of autophagic vacuoles by inhibiting fusion between autophagosomes and lysosomes in rat hepatoma cell line, H-4-II-E cells. Cell Struct. Funct. 23 (1), 33–42.
Yano, M., Kanazawa, M., Terada, K., et al., 1997. Visualization of mitochondrial protein import in cultured mammalian cells with green fluorescent protein and effects of overexpression of the human import receptor Tom20. J. Biol. Chem. 272 (13), 8459–8465.
Yoshii, S.R., Kishi, C., Ishihara, N., et al., 2011. Parkin mediates proteasome-dependent protein degradation and rupture of the outer mitochondrial membrane. J. Biol. Chem. 286 (22), 19630–19640.
Zhang, X., Yuan, Y., Jiang, L., et al., 2014. Endoplasmic reticulum stress induced by tunicamycin and thapsigargin protects against transient ischemic brain injury: involvement of PARK2-dependent mitophagy. Autophagy 10 (10), 1801–1813.